Neuropilin-1 mediates myeloid cell chemoattraction and influences retinal neuroimmune crosstalk

Agnieszka Dejda,[1,2] Gaelle Mawambo,[1] Agustin Cerani,[1] Khalil Miloudi,[3] Zhuo Shao,[1] Jean-Francois Daudelin,[4] Salix Boulet,[4] Malika Oubaha,[3] Felix Beaudoin,[1] Naoufal Akla,[2] Sullivan Henriques,[2] Catherine Menard,[1] Andreas Stahl,[5] Jean-Sébastien Delisle,[4] Flavio A. Rezende,[2] Nathalie Labrecque,[4] and Przemyslaw Sapieha[1,2,3]

[1]Department of Biochemistry and Molecular Medicine and [2]Department of Ophthalmology, Maisonneuve-Rosemont Hospital Research Centre, University of Montreal, Montreal, Quebec, Canada. [3]Department of Neurology and Neurosurgery, McGill University, Montreal, Quebec, Canada. [4]Department of Medicine Microbiology, Infectiology and Immunology, Maisonneuve-Rosemont Hospital Research Centre, University of Montreal, Montreal, Quebec, Canada. [5]University Eye Hospital Freiburg, Freiburg, Germany.

Immunological activity in the CNS is largely dependent on an innate immune response and is heightened in diseases, such as diabetic retinopathy, multiple sclerosis, amyotrophic lateral sclerosis, and Alzheimer's disease. The molecular dynamics governing immune cell recruitment to sites of injury and disease in the CNS during sterile inflammation remain poorly defined. Here, we identified a subset of mononuclear phagocytes (MPs) that responds to local chemotactic cues that are conserved among central neurons, vessels, and immune cells. Patients suffering from late-stage proliferative diabetic retinopathy (PDR) had elevated vitreous semaphorin 3A (SEMA3A). Using a murine model, we found that SEMA3A acts as a potent attractant for neuropilin-1–positive (NRP-1–positive) MPs. These proangiogenic MPs were selectively recruited to sites of pathological neovascularization in response to locally produced SEMA3A as well as VEGF. NRP-1–positive MPs were essential for disease progression, as NRP-1–deficient MPs failed to enter the retina in a murine model of oxygen-induced retinopathy (OIR), a proxy for PDR. OIR mice with NRP-1–deficient MPs exhibited decreased vascular degeneration and diminished pathological preretinal neovascularization. Intravitreal administration of a NRP-1–derived trap effectively mimicked the therapeutic benefits observed in mice lacking NRP-1–expressing MPs. Our findings indicate that NRP-1 is an obligate receptor for MP chemotaxis, bridging neural ischemia to an innate immune response in neovascular retinal disease.

Introduction

The CNS had long been considered an immune-privileged system, yet it is now clear that the brain, retina, and spinal cord are subjected to complex immune surveillance (1, 2). This is evident in the retina, in which an intensified, largely microglial/macrophage-based immune response is associated with the progression of several sight-threatening diseases, such as diabetic retinopathy (DR) (3–5), age-related macular degeneration (AMD) (6–8), and retinopathy of prematurity (ROP) (9, 10). Together, these retinal diseases account for the principal causes of loss of sight in industrialized countries (6, 11, 12).

A common etiology for blinding vasoproliferative retinopathies such as DR and ROP is the initial degeneration of retinal microvasculature, followed by ischemic stress on the neuroretina. This triggers a second phase of deregulated and destructive angiogenesis (13). Given this sequence of events and prominent clinical features, the most widely used, current local ocular therapeutic interventions directly target pathological neovascularization yet present a number of nondesirable off-target effects. For exam-

ple, front-line treatments, such as laser photocoagulation, which ablate ischemic retinal tissue with the aim of reducing production of angiogenic factors, compromise visual field and provoke scotomas. Moreover, given the neurosupportive properties of VEGF, a growing number of neurological and developmental side effects are being attributed to long-term intravitreal anti-VEGFs regimens (4, 11, 14–16). Overcoming these therapeutic limitations or exploring novel pharmacological avenues is therefore required to ameliorate the safety profiles of current interventions. In this regard, there is increasing evidence for the breakdown of the neurovascular unit in proliferative retinopathies (4, 17, 18). In particular, retinal ganglion cells and neurons of the inner nuclear layer that are in intimate contact with degenerating vasculature in DR and ROP (Supplemental Figure 1; supplemental material available online with this article; doi:10.1172/JCI76492DS1) are subjected to various forms of cellular stress, including ER stress (19), oxidative stress (13), inflammatory stress (18–21), and increased microglial activity (22–25). Whether stressed or damaged central retinal neurons themselves have the propensity to modulate the immune response to reestablish local homeostasis, clear debris (2), or segregate irreparably damaged tissue (17) is unknown and could provide therapeutic insight for designing targeted inhibitors of sterile neuroinflammation.

While a role for mononuclear phagocytes (MPs), such as microglia/macrophages, has been established in proliferative retinopathies (22–25), the local tissue-specific molecular cues and
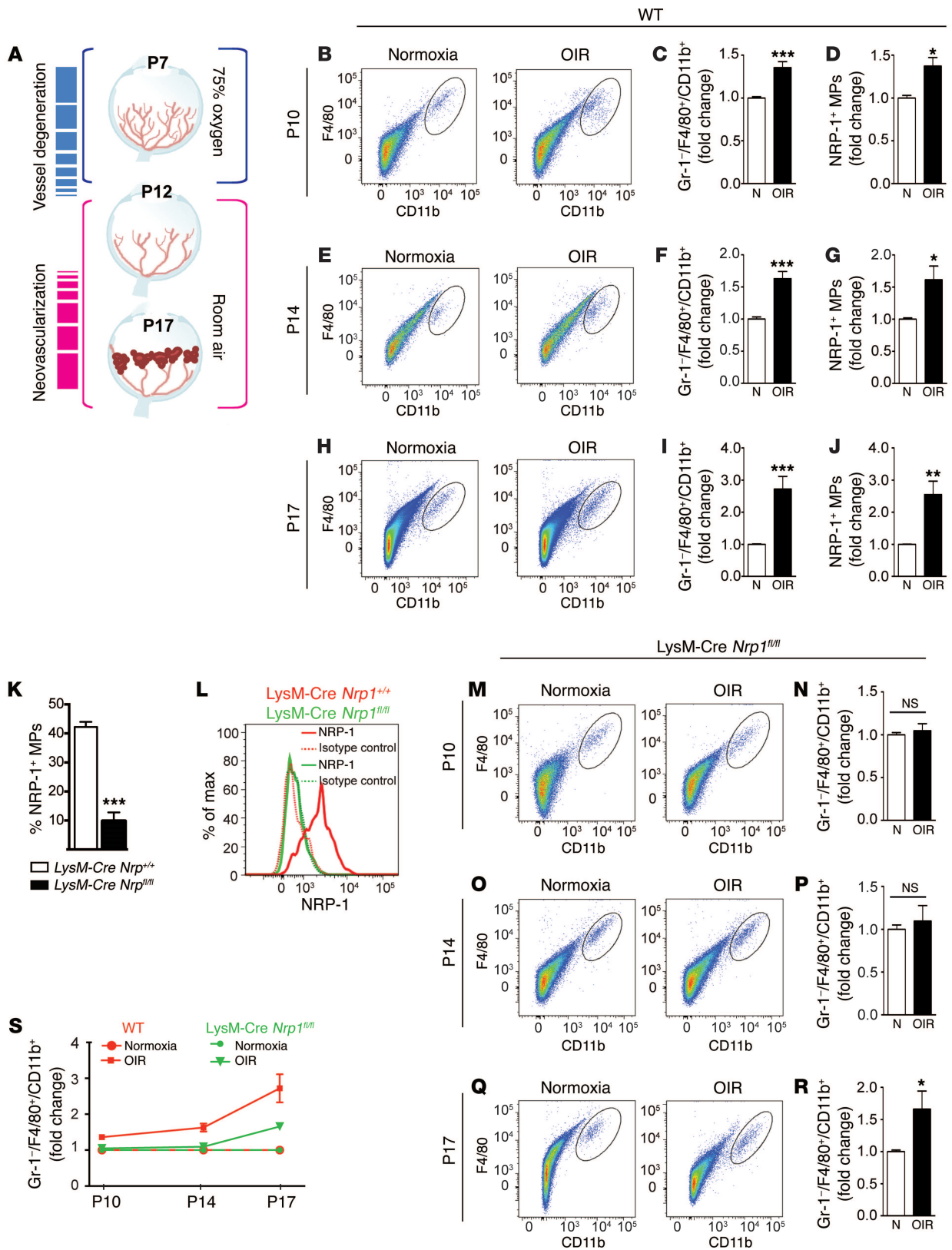
Figure 1. NRP-1 identifies a population of MPs that are mobilized secondary to vascular injury. (**A**) Schematic depiction of the mouse model of OIR. Representative FACS plots of Gr-1⁻/F4/80⁺/CD11b⁺ cells (microglia) in retinas collected at (**B**) P10, (**E**) P14, and (**H**) P17 from WT OIR and normoxic (N) control mice. (**C**, **F**, and **I**) The number of retinal microglia was significantly increased in OIR at all points analyzed; *n* = 7–8 (normoxic and OIR) (total of 28–32 retinas per condition; each "*n*" comprises 4 retinas). (**D**, **G**, and **J**) A proportional increase in the number of NRP-1⁺ microglia was observed in OIR retinas; *n* = 3–5 (normoxic and OIR) (total of 12–20 retinas per condition; each "*n*" comprises 4 retinas). (**K** and **L**) To investigate the role of MP-resident NRP-1, we generated LysM-Cre *Nrp1ᶠˡ/ᶠˡ* mice, which have significantly compromised *Nrp1* expression in retinal microglia; *n* = 3 (WT), *n* = 4 (LysM-Cre *Nrp1ᶠˡ/ᶠˡ*) (total of 12–16 retinas per condition). (**M** and **O**) FACS analysis at P10 and P14 during the proliferative phase of OIR reveals that MP-resident NRP-1 is essential for MP infiltration into the ischemic retina, (**N** and **P**) as LysM-Cre *Nrp1ᶠˡ/ᶠˡ* mice did not show an increase in numbers of Gr-1⁻/F4/80⁺/CD11b⁺ cells in OIR at these time points. (**Q** and **R**) At P17, MPs infiltrate independent of NRP-1; *n* = 7–8 (normoxic), *n* = 7–9 (OIR) (total of 28–36 retinas per condition; each "*n*" comprises 4 retinas). (**S**) MP accumulation in the retinas over the course of OIR in WT and LysM-Cre *Nrp1ᶠˡ/ᶠˡ* mice. Data is expressed as fold change relative to control ± SEM. *$P < 0.05$, **$P < 0.001$, ***$P < 0.0001$.

mechanisms of chemoattraction by which these cells are called to partake in or respond to neuroretinal injury remain largely ill defined. We therefore addressed this question with the widely used mouse model of oxygen-induced retinopathy (OIR) that mimics the destructive vasoproliferative phase of ocular neovascular diseases, such as DR (26). A candidate receptor that could bridge neuronal stress to an immune response is neuropilin-1 (NRP-1). This single-pass transmembrane receptor, with a large 860–amino acid extracellular domain, has the unconventional ability to bind at least 2 structurally unrelated ligands (VEGF₁₆₅ and semaphorin 3A [SEMA3A]) via distinct sites (27–29). While predominantly recognized for its role in neuronal or vascular guidance and as a coreceptor for VEGF₁₆₅ (30), it has also been

described on microglia during vascular anastomosis (31) and recently described in tumor-associated macrophages with roles in vessel maturation (32) and proangiogenic properties (33). Importantly, the physiological role of myeloid-resident NRP-1 remains unclear, particularly in the context of the CNS. We therefore sought to determine the function of myeloid-resident NRP-1 in the pathogenesis of proliferative retinopathies.

Here, we demonstrate that, via production of SEMA3A and VEGF, the ischemic neural retina has the inherent capacity to modulate the innate immune response by summoning circulating MPs to sites of vascular injury. We provide evidence in both human and animal studies for the critical role of myeloid-resident NRP-1 in the chemotaxis and accretion of MPs in proliferative retinopathies. Our findings further suggest that current anti-VEGF therapies may in part be effective by reducing destructive ocular inflammation.

Results

NRP-1 identifies a population of MPs that are mobilized secondary to vascular injury. To determine whether MPs such as microglia or macrophages partake in the vascular pathogenesis associated with proliferative retinopathies, we first carried out FACS analysis on whole mouse retinas to elucidate the kinetics of macrophage/microglial accumulation throughout the evolution of OIR (Figure 1A) (75% oxygen from P7–P12 to induce vaso-obliteration and room air until P17 to attain maximal preretinal neovascularization) (refs. 26, 33, and Figure 1, B, E, and H). Our data revealed significantly higher numbers of retinal macrophage/microglial cells (Gr-1⁻, F4/80⁺, CD11b⁺ cells) (gating scheme in Supplemental Figure 2) in OIR at all time points analyzed, including a 36% increase during the vaso-obliterative phase at P10 ($P = 0.0004$) (Figure 1C), a 63% rise during the neovascular phase at P14 ($P < 0.0001$) (Figure 1F), and a 172% surge during maximal neovascularization at P17 ($P = 0.0006$) (Figure 1I). These findings agree with the prevailing notion of microglial involvement in retinal neovascularization (22, 23, 34).
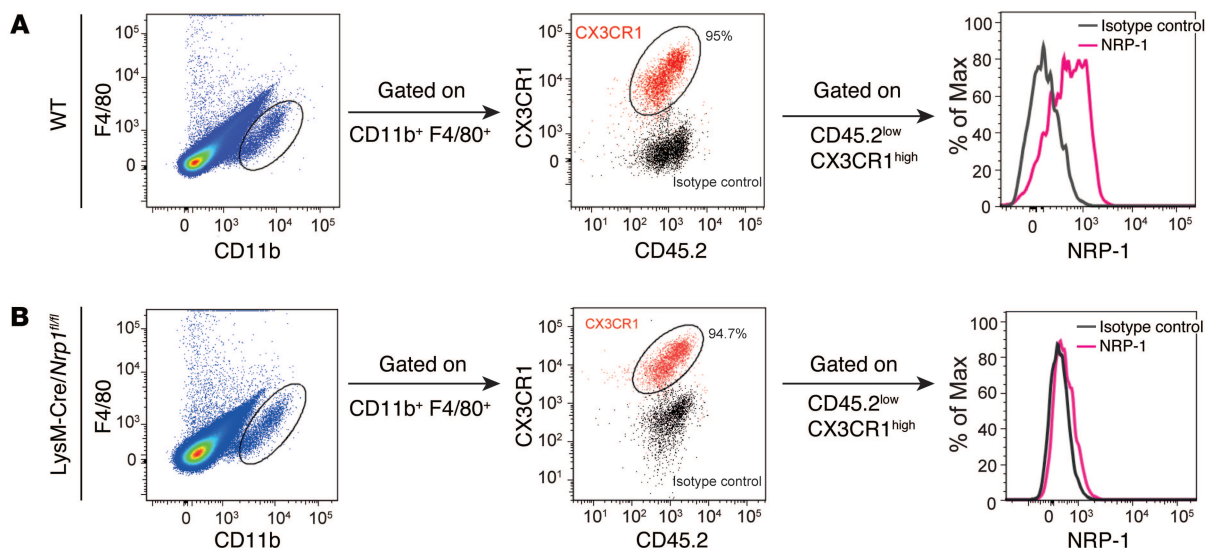

Figure 2. Retinal NRP-1⁺ MPs express microglial markers. Representative FACS plots from P14 OIR retinas depicting that (**A**) 95% (in WT) and (**B**) 94.7% (in LysM-Cre *Nrp1ᶠˡ/ᶠˡ*) of Gr-1⁻/F4/80⁺/CD11b⁺ cells express high levels of CX3CR1 and intermediate/low levels of CD45 consistent with a microglial phenotype. CX3CR1ʰⁱ and CD45ˡᵒ cells (**A**) express NRP-1 in WT retinas and (**B**) do not express NRP-1 in retinas from LysM-Cre *Nrp1ᶠˡ/ᶠˡ* mice.
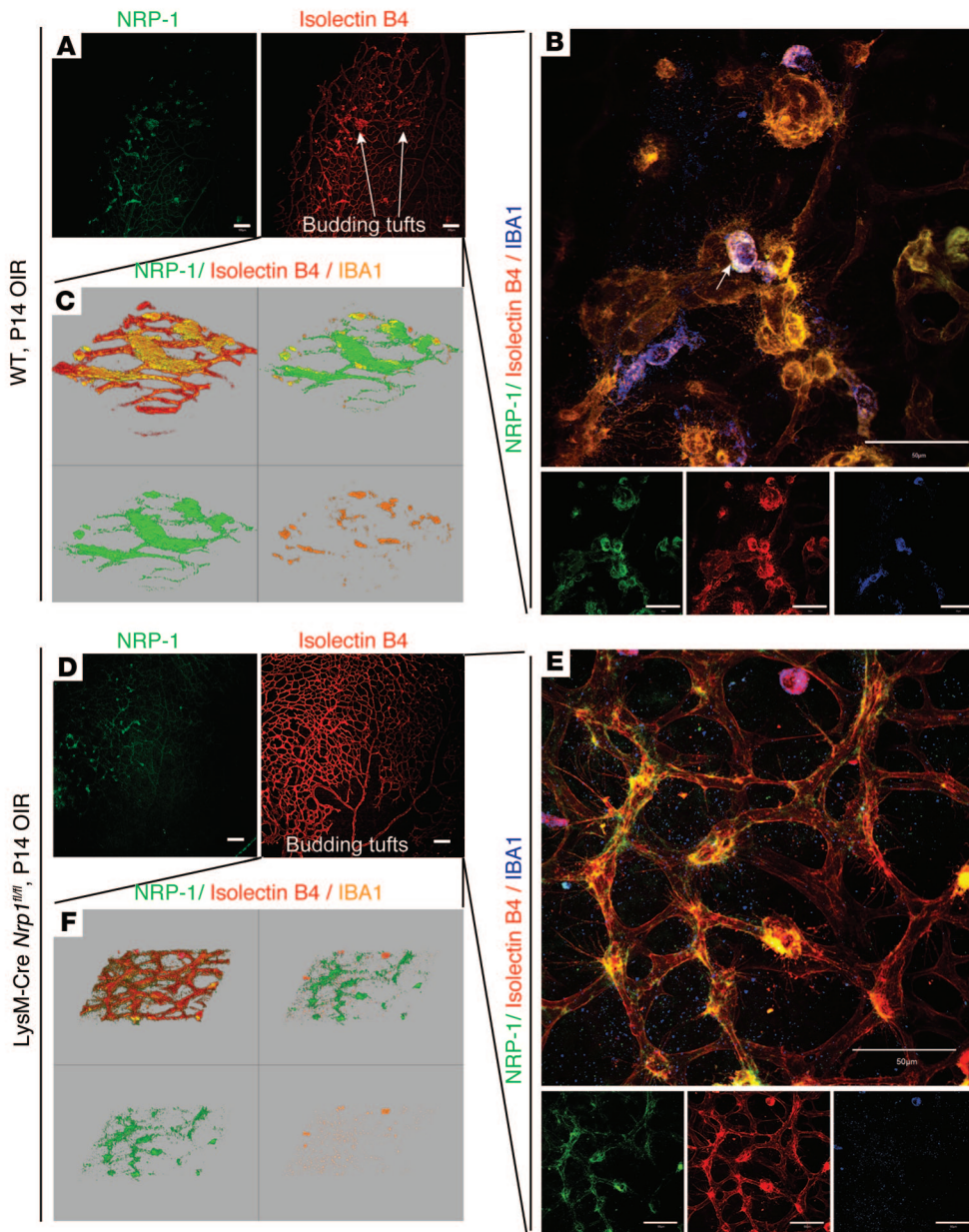
Figure 3. NRP-1+ myeloid cells localize to sites of pathological neovascularization in the retina. Confocal images of isolectin B4– (vessel and microglia stain) and NRP-1–stained retinal flat mounts at P14 with budding neovascular tufts in (**A**) WT and (**D**) LysM-Cre *Nrp1*fl/fl mice. (**B**) High-magnification images reveal colocalization of NRP-1+ microglia (IBA1) with nascent tufts. (**D–F**) LysM-Cre *Nrp1*fl/fl mice had fewer MPs and fewer developed tufts. (**C** and **F**) Observations where confirmed by 3D reconstruction. White arrows in **A** point to nascent sprouting tufts. The white arrow in **B** points to NRP-1+ MPs associated with growing tufts. For all immunohistochemistry images, representative images of 3 independent experiments are shown. Scale bars: 100 μm (**A** and **D**); 50 μm (**B** and **E**).

Importantly, at each time point investigated, we observed a proportional increase in NRP-1+ MPs in OIR, with a rise of 37% at P10 (*P* = 0.0240) (Figure 1D), 61% at P14 (*P* = 0.0196) (Figure 1G), and 155% at P17 (*P* = 0.0058) (Figure 1J), suggesting that this subpopulation of NRP-1+ MPs was being recruited to the neuroretina during the progression of the disease. For all OIR experiments, weights of mouse pups were recorded (Supplemental Figure 3) to ascertain adequate metabolic health (35).

In order to establish the role of MP-resident NRP-1 in retinopathy, we generated a myeloid-specific knockout of *Nrp1* by intercrossing *Nrp1*-floxed mice with LysM-Cre mice (36), yielding LysM-Cre *Nrp1*fl/fl progeny. The resulting mice showed an approximately 80% decrease in NRP-1 expression in retinal MPs when compared with that in LysM-Cre *Nrp1*+/+ littermate controls (*P* = 0.0004) (Figure 1, K and L). Of note, mice tested negative for the *rd8* mutation of the *Crb1* gene (37). LysM-Cre *Nrp1*fl/fl mice did not show any difference in body weight, size, or open-field activity when compared with littermates throughout the period of experimentation (from P1–P17) (data not shown) and had similar numbers of resident retinal microglia (Supplemental Figure 4). Remarkably, deletion of NRP-1 on myeloid cells fully abrogated the entry of macrophages/microglia at P10 and P14 OIR (Figure 1, M–P), revealing the critical role for this receptor in MP chemotaxis during the early stages of ischemic retinal injury. At P17, following maximal pathological neovascularization, MP infiltration occurred largely independent of NPR-1 (Figure 1, Q–S). Consistent with a potential microglial identity, the NRP-1–expressing Gr-1–/F4/80+/CD11b+ cells identified above expressed high levels of CX3CR1 and intermediate/low levels of CD45 (Figure 2A). A comparison with spleen-derived cells is provided in Supplemental Figure 5. As expected, in LysM-Cre *Nrp1*fl/fl retinas, CX3CR1hi/CD45lo MPs were devoid of NRP-1 (Figure 2B).

NRP-1+ myeloid cells localize to sites of pathological neovascularization in the retina. Given the pronounced influx of NRP-1+ macro-
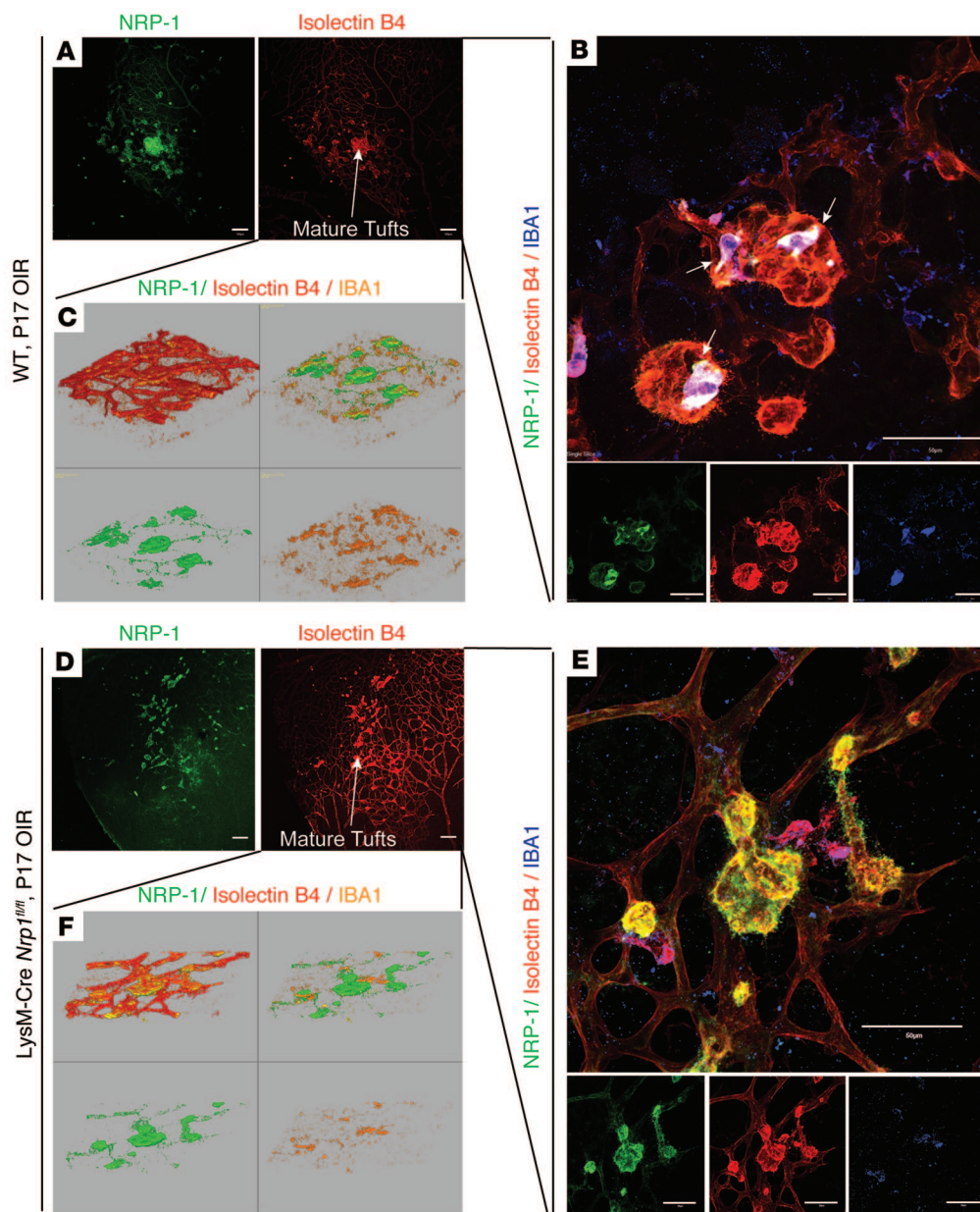
Figure 4. NRP-1+ myeloid cells are associated with pathological neovascular tufts. Confocal images of isolectin B4– (vessel and microglia stain) and NRP-1–stained retinal flat mounts at P17 during maximal neovascularization in (**A**–**C**) WT and (**D**–**F**) LysM-Cre *Nrp1*fl/fl mice. In WT retinas, NRP-1+ microglia (IBA1) associate with mature tufts. (**C** and **F**) Images were reconstructed in 3D. White arrows in **A** and **D** point to mature tufts. White arrows in **B** point to NRP-1+ MPs associated with mature tufts. (**D**–**F**) LysM-Cre *Nrp1*fl/fl mice had fewer MPs and less tufting. For all immunohistochemistry images, representative images of 3 independent experiments are shown. Scale bars: 100 μm (**A** and **D**); 50 μm (**B** and **E**).

phage/microglia during OIR, we next sought to determine where these cells localize during the progression of disease. Immunofluorescence on retinal flat mounts revealed that NRP-1+ macrophage/microglia (colabeled with IBA1 and NRP-1) were intimately associated with nascent pathological tufts at P14 of OIR (Figure 3, A–C) as well as mature tufts at P17 of OIR (Figure 4, A–C). White arrows in Figure 3B and Figure 4B point to NRP-1+ MPs associated with preretinal tufts. NRP-1 was also expressed by endothelial cells on the endothelium of neovascular tufts as previously reported (21). Consistent with data presented in Figure 1, LysM-Cre *Nrp1*fl/fl mice had lower numbers of macrophage/microglia and less pronounced neovascularization (see below for full quantification) (Figure 3, D–F, and Figure 4, D–F).

SEMA3A is elevated in the vitreous of patients suffering from active proliferative DR. To establish the clinical relevance of our findings on the obligate role of NRP-1 in MP chemotaxis in retinopathy, we investigated the concentrations of SEMA3A directly

in the vitreous of patients suffering from active proliferative DR (PDR). Seventeen samples of undiluted vitreous were obtained from patients suffering from active PDR, and seventeen samples were obtained from control patients with nonvascular pathology. Detailed characteristics of patients are included in Table 1. Control patients presented with nonvascular pathology and showed signs of non-diabetes–related retinal damage, such as tractional tension on vasculature (Figure 5, A and B, white arrows) secondary to fibrotic tissue and macular bulging (Figure 5C). In contrast, all retinas from patients with PDR showed signs of disc (Figure 5D) or preretinal neovascularization (Figure 5F), with highly permeable microvessels (leakage of fluorescent dye) (Figure 5, D and G), microaneurysms (Figure 5, D–G), and fibrous scar tissue, indicative of advanced retinopathy (Figure 5G). In addition, patients showed some evidence of macular edema due to compromised vascular barrier function, including cystoid formation due to focal coalescence of extravasated fluid (Figure 5H).

Table 1. Characteristics of patients having undergone vitreous biopsy

Sample	Age (yr)	Diabetes type	Duration (yr)	Retinopathy	Analysis
C1	74	NA	NA	MH	WB/ELISA
C2	54	NA	NA	MMD	WB/ELISA
C3	72	NA	NA	ERM	WB/ELISA
C4	77	NA	NA	ERM	WB/ELISA
C5	82	NA	NA	MH	WB/ELISA
C6	62	NA	NA	ERM	ELISA
C7	65	NA	NA	MH	ELISA
C8	69	NA	NA	ERM	ELISA
C9	75	NA	NA	MH/cataract	ELISA
C10	77	NA	NA	Ret.Det.	ELISA
C11	69	NA	NA	ERM	ELISA
C12	68	NA	NA	ERM	ELISA
C13	81	NA	NA	ERM	ELISA
C14	70	NA	NA	ERM	ELISA
C15	65	NA	NA	MH	ELISA
C16	74	NA	NA	MH	ELISA
C17	75	NA	NA	MH	ELISA
PDR1	62	2	13	PDR	WB/ELISA
PDR2	79	2	33	PDR	WB/ELISA
PDR3	73	2	15	PDR	WB/ELISA
PDR4	74	2	10	PDR	WB/ELISA
PDR5	54	1	20	PDR	WB/ELISA
PDR6	60	2	34	PDR	WB/ELISA
PDR7	77	2	34	PDR	WB/ELISA
PDR8	71	2	10	PDR	ELISA
PDR9	35	–	–	PDR	ELISA
PDR10	69	2	40	PDR	ELISA
PDR11	78	–	5	PDR	ELISA
PDR12	36	2	–	PDR	ELISA
PDR13	81	1	30	PDR	ELISA
PDR14	70	2	30	PDR	ELISA
PDR15	74	–	35	PDR	ELISA
PDR16	67	2	30	PDR	ELISA
PDR17	69	2	2	PDR	ELISA

MH, macular hole; MMD, myopic macular degeneration; ERM, epiretinal membrane; Ret.Det., retinal detachment; WB, Western blot; NA, not applicable; –, not available.

Consistent with a role in PDR, ELISA-based detection of SEMA3A revealed a 5-fold higher concentration of the protein in the vitreous humors of patients with PDR when compared with that in the vitreous of control patients ($P = 0.0132$) (Figure 5I). Results were confirmed by Western blot analysis on equal volumes of vitreous, where SEMA3A (125- and 95-kDa isoforms) (38, 39) was elevated in patients with PDR (Figure 5J). Thus, upregulation of SEMA3A in the vitreous is induced in diabetic ocular pathology.

NRP-1 ligands are induced in the retinal ganglion cell layer during OIR. To obtain an accurate kinetic profile of expression of the 2 prominent ligands of NRP-1 in proliferative retinopathy, we investigated levels of *Sema3a* and *Vegf* message in the mouse model of OIR. Real-time quantitative PCR (RT-qPCR) on whole retinas revealed that *Sema3a* was robustly induced in OIR both during the hyperoxic (vasodegenerative) phase at P10 and the ischemic/neovascular stage from P12 to P17 (Figure 6A). The observed induction occurred in both WT and LysM-Cre *Nrp1$^{fl/fl}$* retinas. Con-

versely, as expected, *Vegf* transcripts rose exclusively in the ischemic phase of OIR from P12 to P17 (Figure 6B). Importantly, *Vegf* was significantly less induced in LysM-Cre *Nrp1$^{fl/fl}$* retinas when compared with WT retinas (minimally increased at P12; $P = 0.0451$) and approximately 55% lower at P14 when compared WT OIR ($P = 0.0003$) (Figure 6B), indicative of a healthier retina.

We next performed laser capture microdissection followed by RT-qPCR on retinal layers in avascular zones to pinpoint the source of *Sema3a* and *Vegf* message in OIR (Figure 4C). Both *Sema3a* and *Vegf* were robustly induced in the ganglion cell layer, with *Vegf* also increasing in the inner nuclear layer (Figure 6, D and E). Thus, the source of both ligands is geographically consistent with the localization of retinal MPs (Figures 3 and 4).

MPs do not proliferate in the retina after vascular injury. In order to determine whether the noted rise in NRP-1$^+$ MPs was due to an influx from systemic circulation or an increase in MP proliferation within the retina, we investigated local retinal proliferation of these cells. Mice were systemically injected with BrdU at P13 (24 hours prior to sacrifice), and FACS analysis was carried out on retinas (Figure 7A) and spleens (Figure 7B). Within the retinas, Gr-1$^-$/F4/80$^+$/CD11b$^+$ MPs did not show significant proliferation ($P = 0.4708$). Considerably more proliferation was observed in spleens. No significant difference was observed between normoxia and OIR (Figure 7C). The lack of proliferation of MPs in the retinas suggests that the noted accretion of NRP-1$^+$ MPs during retinopathy has a systemic or bone marrow–derived origin, as previously elegantly demonstrated for proangiogenic macrophages (40, 41).

SEMA3A and VEGF$_{165}$ mobilize MPs via NRP-1. In light of the requirement of NRP-1 for myeloid cell mobilization to sites of vascular lesion (Figure 1) as well as the induction of the principal ligands of NRP-1 in retinopathy (Figures 5 and 6) and the likely systemic origin of these cells (Figure 7), we sought to determine the propensity of these cues to provoke chemotaxis of MPs. Primary macrophage cultures were isolated from WT mice and subjected to a Transwell Boyden chamber migration assay. Both SEMA3A (100 ng/ml) ($P < 0.0001$) and VEGF$_{165}$ (50 ng/ml) ($P = 0.0027$) provoked macrophage chemotaxis to similar magnitudes as positive control MCP-1 (100 ng/ml) ($P < 0.0001$) (Figure 8, A and B). These data were validated by demonstrating that Y-27632, a selective inhibitor Rho-associated coiled coil–forming protein serine/threonine kinase (ROCK), abolished their chemotactic properties. ROCK is downstream of NRP-1 signaling (42) and is known to mediate monocyte migration (43). VEGF migration was partially yet not significantly diminished, suggesting a contribution from alternate receptors such as VEGFR1 as recently reported (33). Consistent with a role for NRP-1 in SEMA3A- and VEGF-mediated chemotaxis, macrophages from LysM-Cre
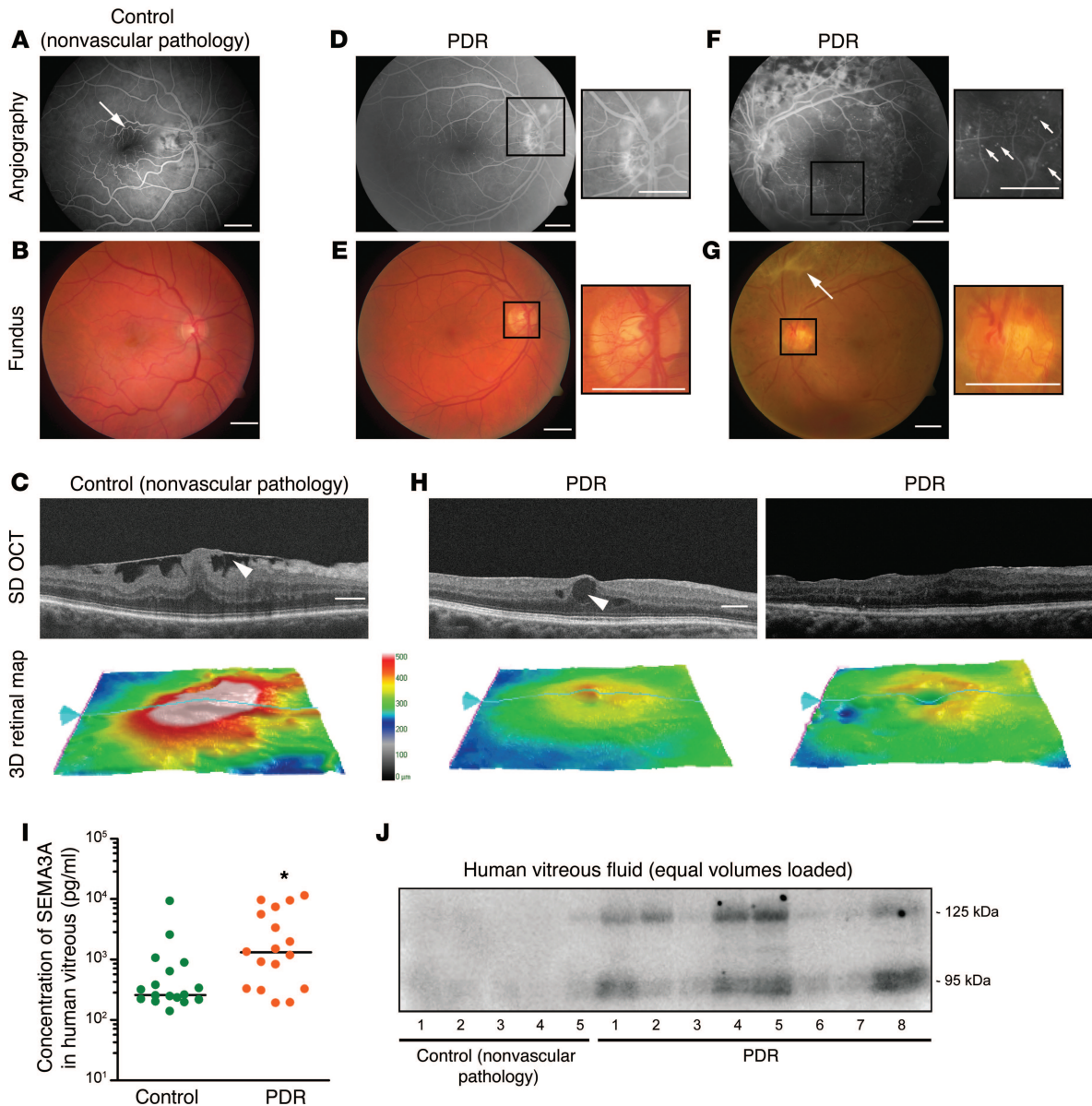
Figure 5. The NRP-1 ligand SEMA3A is induced in patients suffering from PDR. Angiographies, funduscopies, spectral-domain optical coherence tomography (SD-OCT), and 3D retinal maps obtained from patients selected for the study. Control patients had nonvascular pathologies and were compared with patients with PDR. Control patients with epiretinal membrane shows signs of non-diabetes–related retinal damage, such as (**A** and **B**) tractional tension on vasculature (arrow) secondary to (**C**) fibrotic tissue (white arrow) and macular bulging (angiography and 3D map). Retinas from patients with PDR have (**E**) neovascularization (high-magnification image) with (**D**) highly permeable microvessels, as evidenced by leakage of fluorescent dye (high-magnification image), (**F**) microaneurysms (arrows in high-magnification image), and (**G**) fibrous scar tissue (arrow), indicative of advanced retinopathy. (**H**) Patients with PDR show some evidence of macular edema, including cystoid formation (white arrowhead) due to focal coalescence of extravasated fluid. (**I**) Vitreous humor analyzed by ELISA shows 5-fold increased levels of SEMA3A protein in patients with PDR. Horizontal bars represent mean concentration of SEMA3A, and dots represent concentrations of individual samples; $n = 17$ for controls and 17 for patients with PDR; *$P < 0.05$. (**J**) Western blot analysis of equal volumes of vitreous corroborates the increase in SEMA3A (~125 KDa and 95 KDa) in patients with PDR with respect to controls. Scale bars: 1,500 μm (**A**–**G**); 300 μm (**C** and **H**).

Nrp1^{fl/fl} mice were uniquely responsive to MCP-1 and not mobilized by SEMA3A or VEGF (Figure 8C).

NRP-1⁺ macrophages potentiate microvascular sprouting ex vivo. To investigate the impact of NRP-1 expressing macrophages on microvascular angiogenesis, we isolated choroid tissue from either LysM-Cre *Nrp1^{+/+}* mice or LysM-Cre *Nrp1^{fl/fl}* mice and grew them in Matrigel to assess microvascular sprouting. Chor-

oids from LysM-Cre *Nrp1^{fl/fl}* mice sprouted approximately 20% fewer microvessels when compared with ones from LysM-Cre *Nrp1^{+/+}* mice ($P = 0.018$) (Figure 9A). To investigate the role of NRP-1⁺ macrophages in promoting microvascular sprouting, we used clodronate liposomes to eliminate endogenous macrophages from the isolated choroid tissues. In explants from both LysM-Cre *Nrp1^{fl/fl}* and LysM-Cre *Nrp1^{+/+}* mice, PBS containing
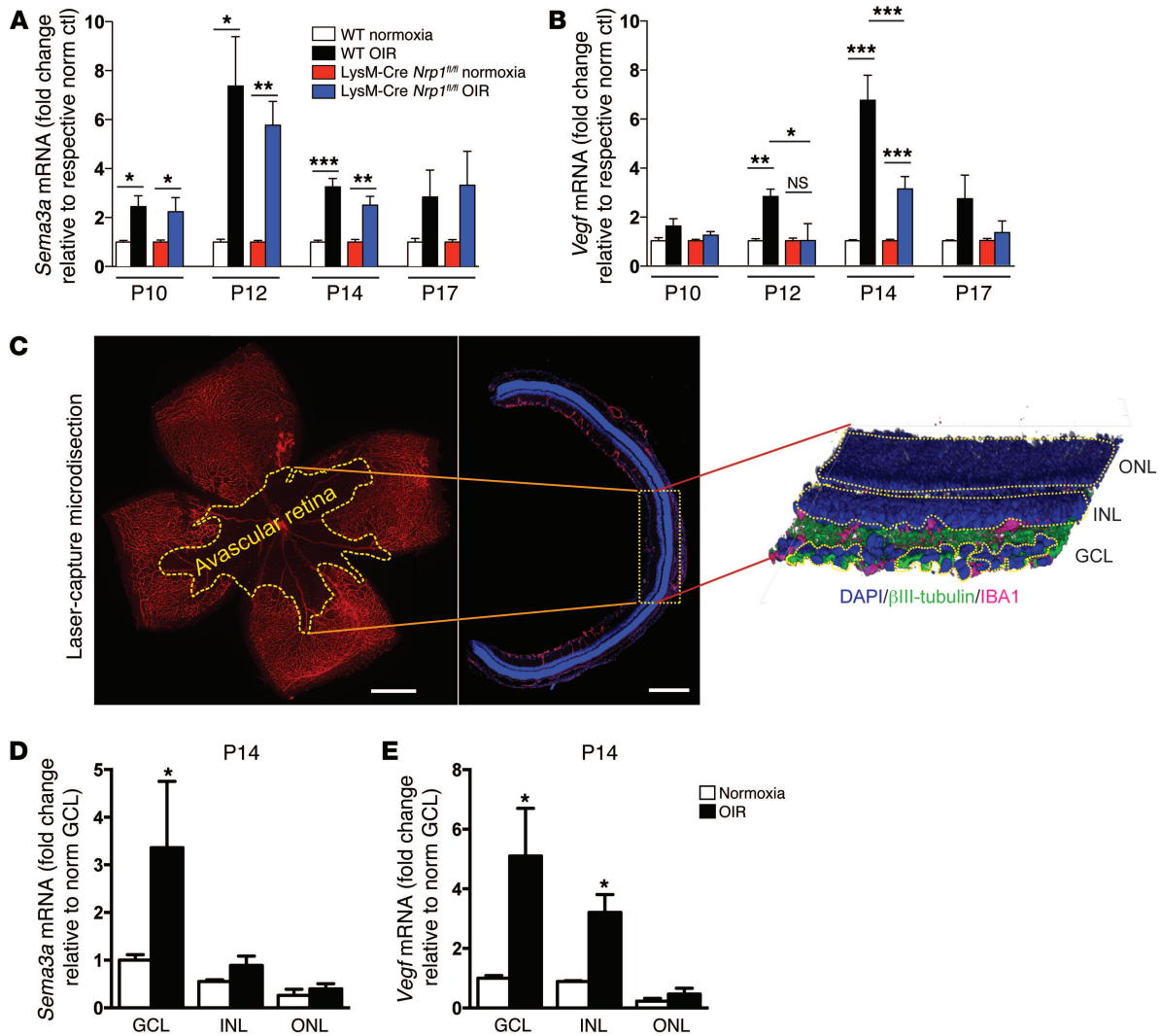
Figure 6. Ligands of NRP-1 are induced in the retinal ganglion cell layer during OIR. (A and B) Retinas from WT and LysM-Cre *Nrp1*^{fl/fl} mice under normoxic conditions or in OIR were collected between P10 and P17 and analyzed by RT-qPCR. **(A)** *Sema3a* mRNA expression was induced throughout OIR in both WT and LysM-Cre *Nrp1*^{fl/fl} retinas, **(B)** while *Vegf* was significantly less induced in LysM-Cre *Nrp1*^{fl/fl} retinas compared with WT retinas. Data are expressed as a fold change relative to respective normoxic controls for each time point ± SEM; *n* = 4–7; *P < 0.05, **P < 0.01, ***P < 0.001. **(C)** Laser capture microdissection was performed on P14 mice, with care being taken to select avascular retinal zones in OIR. RT-qPCR on laser capture microdissection of retinal layers in control and OIR avascular zones showed an induction in both **(D)** *Sema3a* and **(E)** *Vegf* mRNA in the ganglion cell layer (GCL) in OIR retinas compared with normoxic retinas. **(E)** *Vegf* was also induced in the inner nuclear layer (INL) of OIR retinas. ONL, outer nuclear layer. Data are expressed as a fold change relative to normoxic GCL ± SEM. Scale bars: 500 μm **(C;** right); 300 μm **(C;** left).

liposomes (i.e., vehicle control) had no affect on vascular sprouting, but clodronate liposomes reduced microvascular sprouting by approximately 60% (*P* = 0.0114 for LysM-Cre *Nrp1*^{+/+} choroid and *P* = 0.0007 for LysM-Cre *Nrp1*^{fl/fl} choroid) (Figure 9, B–E). To verify whether NRP-1+ macrophages have a propensity to promote angiogenesis, we extracted peritoneal macrophages from LysM-Cre *Nrp1*^{+/+} or LysM-Cre *Nrp1*^{fl/fl} mice and introduced them into choroid explant cultures that had been treated previously with clodronate liposomes and washed. LysM-Cre *Nrp1*^{+/+} macrophages robustly potentiated microvascular sprouting by 50% to 100% when compared with macrophages from LysM-Cre *Nrp1*^{fl/fl} mice (*P* = 0.0068 for LysM-Cre *Nrp1*^{+/+} choroid and *P* = 0.0491 for LysM-Cre *Nrp1*^{fl/fl} choroid) (Figure 9, D and E), independent of the genotype of the choroidal explant.

Deficiency in myeloid-resident NRP-1 reduces vascular degeneration and pathological neovascularization in retinopathy. Given the obligate role of NRP-1 in MP infiltration during the early stages of OIR (Figure 1), we next sought to determine the affect of myeloid cell–specific ablation of NRP-1 on the progression of disease. Upon exit from 75% O₂ at P12, LysM-Cre *Nrp1*^{fl/fl} mice showed significantly lower levels of retinal vaso-obliteration when compared with those of WT (*P* = 0.0011) and LysM-Cre *Nrp1*^{+/+} (*P* < 0.0001) controls (Figure 10, A and B). This may be attributed to lower levels of IL-1β present in the retinas of LysM-Cre *Nrp1*^{fl/fl} mice (Supplemental Figure 6). Importantly, at P17, when pathological neovascularization peaks (26), deletion of myeloid-resident NRP-1 profoundly reduced avascular areas (~35% when compared with WT [*P* < 0.0001] and ~30% compared with LysM-Cre *Nrp1*^{+/+} mice
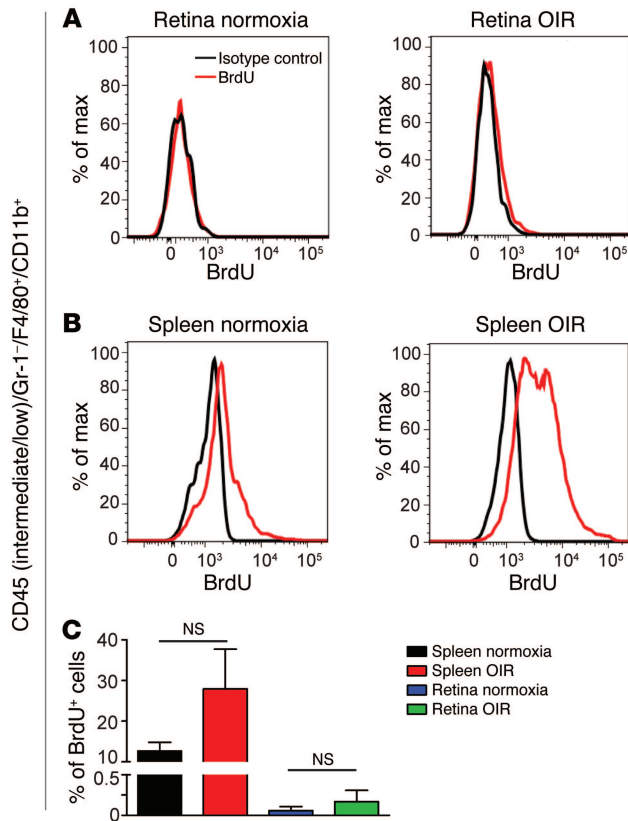
Figure 7. NRP-1⁺ MPs do not proliferate in the retina after vascular injury. Representative FACS histograms of Gr-1⁻/F4/80⁺/CD11b⁺ cells obtained from (**A**) retinas and (**B**) spleens collected at P14 from WT OIR and normoxic control mice injected with BrdU at P13. (**C**) The number of BrdU⁺ cells was considerably higher in spleens but did not change significantly between OIR and normoxic mice; *n* = 4 (normoxic), *n* = 4 (OIR) (total of 16 retinas per condition; each "*n*" comprises 4 retinas). Data are expressed as a percentage of BrdU⁺ Gr-1⁻/F4/80⁺/CD11b⁺ cells ± SEM.

[*P* = 0.0008]) (Figure 10, C and D). In turn, we observed significant reductions in destructive preretinal neovascularization associated with ischemic retinopathy (~36% when compared with WT [*P* = 0.0008] and ~34% compared with LysM-Cre *Nrp1*⁺/⁺ mice [*P* = 0.0013]) (Figure 10, E and F).

Therapeutic intravitreal administration of soluble NRP-1 reduces MP infiltration and pathological neovascularization in retinopathy. To determine the translational potential of our findings, we next used a soluble recombinant mouse NRP-1 (rmNRP-1) (Figure 11A) as a trap to sequester OIR-induced ligands of NRP-1. A single intravitreal injection of rmNRP-1 at P12 lead to a 30% reduction at P14 (*P* = 0.0282) in the number of microglia present in retinas subjected to OIR (Figure 11B). This finding attests to the potency of soluble NRP-1 (1 μl of 500 μg/ml) to compromise microglial mobilization. Intravitreal administration of soluble NRP-1 provoked a significant approximate 40% decrease in pathological preretinal angiogenesis when compared with that of vehicle-injected controls (*P* = 0.0025) (Figure 11, C and D). Together, these data suggest that neutralization of ligands of NRP-1 is an effective strategy to reduce destructive neovascularization in retinopathy.

Discussion

Although the contribution of MPs to ocular neovascular diseases such as DR has been established for over a decade, knowledge of the mechanisms by which they are locally recruited to areas of tissue damage and partake in the disease process remains limited. Here, we demonstrate that stressed retinal neurons (19, 21) and neural tissue have the inherent ability to modulate the local innate immune response via unconventional chemotactic agents, such as

the classical repulsive guidance cue SEMA3A (21) and vasoattractive and neuroattractive VEGF (Figure 12). We provide evidence that these cues act as potent chemoattractants for NRP-1⁺ MPs during the early stages of ischemic injury in the retina and contribute to vascular pathology in retinopathy. This neuroimmune paradigm consolidates the stress-induced neurovascular response to injury with an innate immune response. Either genetic ablation of NRP-1 specifically in myeloid cells (LysM-Cre *Nrp1*ᶠˡ/ᶠˡ) or therapeutic administration of a NRP-1–derived trap limits MP recruitment, reduces vascular degeneration, and decreases destructive pathological neovascularization.

The association of chronic low-grade inflammation with the progression of DR (5) and the link between neonatal infections and ROP (9, 44) underscores the potential therapeutic worth of antiinflammatory drugs in treatment of proliferative retinopathies (45), yet toxicity remains a concern especially in pediatric populations. This is observed with prolonged use of intravitreal glucocorticoids (widely used for diabetic macular edema), which leads to increased cataract formation and elevated intraocular pressure (46). Hence, in order to improve safety profiles of current antiinflammatory treatment paradigms, it will be necessary to provide a honed intervention that specifically targets damaging sterile neuroinflammation.

The identification of the SEMA3A/NRP-1 axis in chemoattraction of destructive MPs in retinopathy may provide such a target. In contrast to VEGF, which is essential for retinal homeostasis, expression of SEMA3A in healthy mature retinas is limited (20). However, in diabetes and OIR, retinal ganglion neurons, which are in intimate proximity with retinal vessels, generate significant amounts of this cue (20, 21). In addition to a role in local MP chemotaxis, SEMA3A also directly affects microvessels (47) and may directly induce endothelial apoptosis and promote cytoskeleton remodeling (47–50). Specifically in the retina, SEMA3A hinders physiological vascular regeneration in OIR (21) and provokes pathological compromise of barrier function in DR (20). Hence, therapeutic neutralization of SEMA3A may provide a multifaceted advantage over current intravitreally delivered compounds and may have limited toxicity, given that its expression is typically restricted to embryogenesis (51). Our data also raise the possibility that, beyond direct influence on angiogenesis and barrier function (52), the mode of action of current anti-VEGF therapies may also in part involve limiting MP-induced lesions to the neuroretina.

Together, the findings presented in this study establish a basis for future investigations on the role of NRP-1⁺ MPs and their ligands in CNS disorders characterized by excessive neuroinflammation. Understanding the signals that influence neuroimmune interplay may provide valuable therapeutic insight for
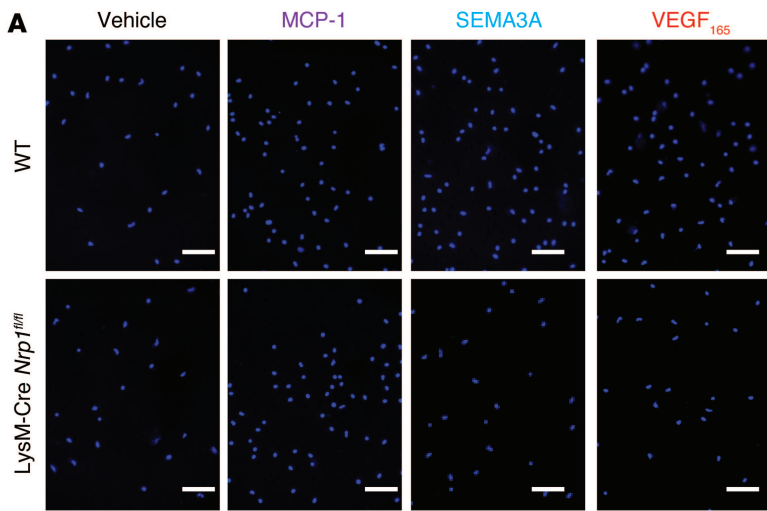
Figure 8. SEMA3A and VEGF are chemoattractive toward macrophages via NRP-1. Primary macrophages were isolated from WT or LysM-Cre *Nrp1*^{fl/fl} mice and subjected to a Transwell migration assay, with vehicle, MCP-1 (100 ng/ml), SEMA3A (100 ng/ml), or VEGF (50 ng/ml) added to the lower chamber. (**A**) Representative images of migrated cells stained with DAPI are shown. (**B**) SEMA3A and VEGF promoted macrophage migration to similar extents as the positive control MCP-1. To ascertain that SEMA3A and VEGF were stimulating macrophage chemotaxis, cells were pretreated with the selective ROCK inhibitor Y-27632 (100 μg/ml), which abolished chemotaxis. (**C**) Macrophages from LysM-Cre *Nrp1*^{fl/fl} mice were unresponsive to SEMA3A or VEGF but responsive to MCP-1. Data are expressed as a fold change relative to control (nontreated cells); horizontal bars represent mean value of the fold change, and dots represent individual fold changes; *n* = 6–22; **P < 0.01, ***P < 0.001. Scale bars: 100 μm.
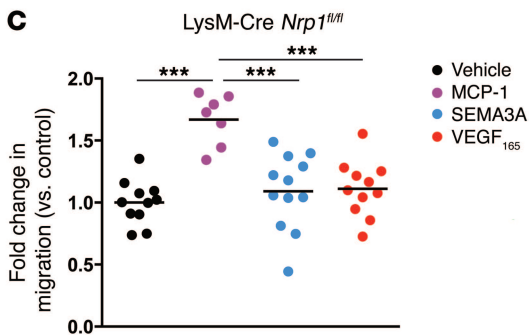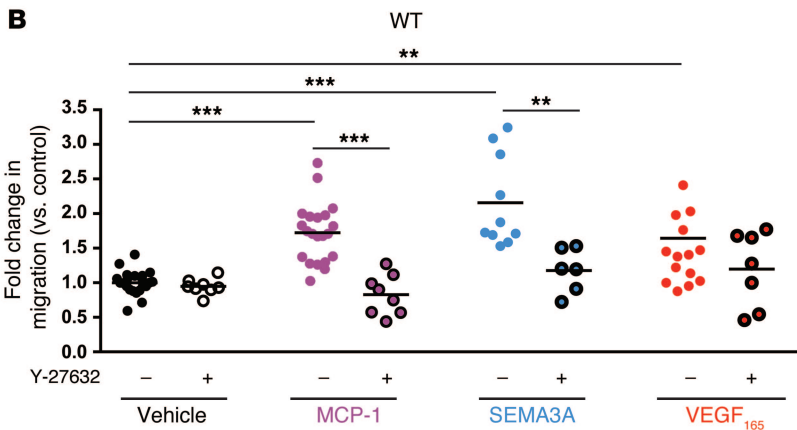
the design of selective antiinflammatory treatments to counter destructive neuroinflammation.

Methods

Animals

C57BL/6 WT mice were purchased from The Jackson Laboratory. LysM-Cre (*Lyz2*[tm1(cre)1fo]/J; no. 004781) and NRP-1–floxed mice (*Nrp1*[tm2Ddg]/J; no. 005247) were purchased from The Jackson Laboratory.

O₂-induced retinopathy

Mouse pups (WT or LysM-Cre [The Jackson Laboratory] or LysM-Cre *Nrp1*^{fl/fl}) and their fostering mothers (CD1, Charles River) were exposed to 75% O₂ from P7 to P12 and returned to room air (53). This

model serves as a proxy to human ocular neovascular diseases such as DR, which is characterized by a late phase of destructive pathological angiogenesis (54, 55). Upon return to room air, hypoxia-driven neovascularization develops from P14 onward (26). We enucleated eyes at different time points and dissected the retinas for FACS analysis or mRNA analysis as described below. In other experiments, dissected retinas were flat mounted and incubated overnight with fluoresceinated isolectin B4 (1:100) in 1 mM CaCl₂ to determine extent of avascular area or neovascularization area at P17 using ImageJ and the SWIFT-neovascularization method (56).

FACS of digested retinas

Retinas from WT or LysM-Cre *Nrp1*^{fl/fl} mice were homogenized and incubated in a solution of 750 U/ml DNase I (Sigma-Aldrich) and 0.5 mg/ml
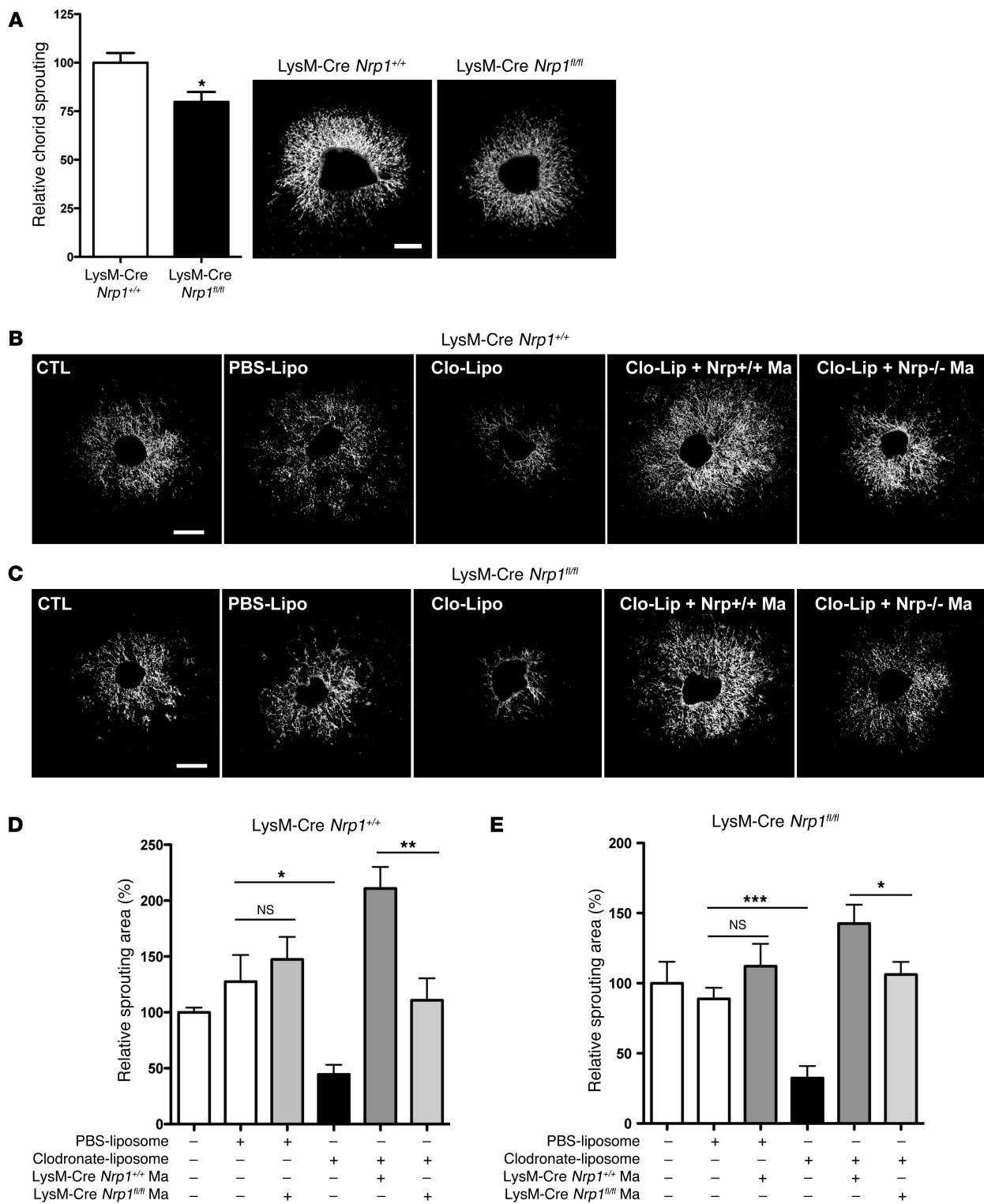
Figure 9. NRP-1+ macrophages promote microvascular growth in ex vivo choroid explants. (**A**) Quantification and representative images of choroid explants isolated from LysM-Cre Nrp1+/+ and LysM-Cre Nrp1fl/fl mice (n = 6; P = 0.018). (**B** and **C**) Representative images of choroid explants from (**B**) LysM-Cre Nrp1+/+ and (**C**) LysM-Cre Nrp1fl/fl mice following clodronate liposome treatment and subsequent addition of exogenous macrophages (Ma). PBS-Lipo, EGM-2 medium with PBS-filled liposome; Clo-Lipo, EGM-2 medium with dichloromethylenediphosphonic acid disodium salt–filled liposome. (**D** and **E**) Quantification of choroidal microvascular sprouting from (**D**) LysM-Cre Nrp1+/+ and (**E**) LysM-Cre Nrp1fl/fl mice depicted in **B** and **C**. PBS-Liposome, EGM-2 medium with PBS-filled liposome; Clodronate-Liposome, EGM-2 medium with dichloromethylenediphosphonic acid disodium salt–filled liposome. (n = 6, *P < 0.05, **P < 0.01, ***P < 0.001). Scale bars: 500 μm.
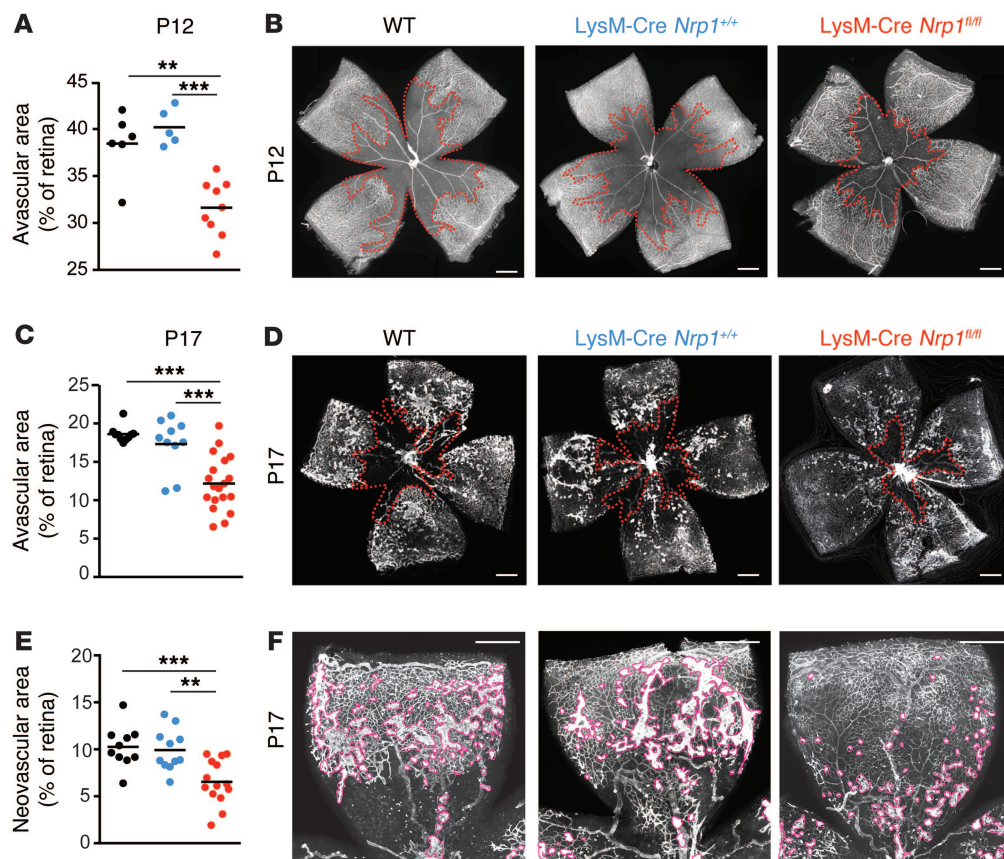
Figure 10. Deficiency in myeloid-resident NRP-1 reduces vascular degeneration and pathological neovascularization in retinopathy. WT, LysM-Cre/*Nrp1*^{+/+}, and LysM-Cre *Nrp1*^{fl/fl} mice were subjected to OIR, and retinas were collected at P12 and P17, flat mounted, and stained with isolectin B4. LysM-Cre *Nrp1*^{fl/fl} mice had (**A** and **B**) less vaso-obliteration at P12 and (**C** and **D**) reduced avascular areas and (**E** and **F**) preretinal neovascularization at P17 compared with both control WT or control LysM-Cre *Nrp1*^{+/+} mice. Results are expressed as percentage of avascular or neovascular area versus the whole retinal area. Horizontal bars represent mean value of percentage, and dots represent individual values; n = 5–19; **$P < 0.01$, ***$P < 0.001$. Scale bars: 250 μm (**B**, **D**, and **F**).

collagenase D (Roche) for 15 minutes at 37°C with gentle shaking. Homogenates were then filtered with a 70-μm cell strainer and washed in PBS and 3% FBS. Spleen samples were homogenized and incubated with 1 mg/ml collagenase D for 10 minutes at 37°C. Homogenates were washed in PBS and 3% FBS, and the pellets were resuspended and incubated in lysis buffer (10 mM $KCHO_3$; 150 mM NH_4Cl; 0.1 mM EDTA) for 5 minutes at room temperature. Cell suspensions (retina or spleen) were incubated with LEAF purified anti–mouse CD16/32 (Biolegend) for 15 minutes at room temperature to block Fc receptors. Cells were then incubated for 30 minutes at room temperature with the following antibodies: FITC anti–mouse/human CD11b (Biolegend), PE/CY7 anti–mouse Ly-6G/Ly-6C (Gr-1; Biolegend), Pacific Blue anti–mouse F4/80 (Biolegend), 7AAD (BD Biosciences), and anti–mNRP-1 allophycocyanin-conjugated rat IgG2A (R&D Systems) or allophycocyanin-conjugated rat IgG2A isotype control (R&D Systems).

For analysis of CX3CR1 and CD45 expression, additional extracellular staining was performed using the above-mentioned antibodies supplemented with Alexa Fluor 700 anti–mouse CD45.2 (Biolegend) and anti–mouse CX3CR1 phycoerythrin-conjugated goat IgG (R&D Systems) or phycoerythrin-conjugated goat IgG isotype control. FACS was performed on a LSRII (BD Biosciences) device, and data were analyzed using FlowJo software (version 7.6.5).

BrdU injections

WT mice subjected to OIR or kept in normoxic conditions were injected intraperitoneally with 5-bromo-2-deoxyuridine (BrdU; Sigma-Aldrich) at the dose of 1 mg per mouse dissolved in PBS at P13.

Analysis of BrdU incorporation

The staining was performed on the retinal cells from P14 WT mice. Samples were obtained as described above. Extracellular staining was performed as described above (CD45.2 [intermediate/low]; Gr-1^{–}; F4/80^{+}, CD11b^{+}; 7AAD). Cells were then fixed with Cytofix/Cytoperm Buffer (BD Biosciences) for 30 minutes and permeabilized with Perm/Wash Buffer (BD Biosciences) for 10 minutes. Next, cells were treated with 300 μg/ml DNAse for 1 hour at 37°C and washed with Perm/Wash Buffer. Intracellular staining of BrdU was performed using anti–BrdU-PE antibodies (Ebioscience) or PE-conjugated mouse IgG1 κ isotype control (Ebioscience) for 25 minutes at 4°C. Cells were then washed in Perm/Wash Buffer and resuspended in PBS and 3% FBS before FACS analysis on a LSRII (BD Biosciences).

Vitrectomy

All patients previously diagnosed with PDR were followed and operated by a single vitreoretinal surgeon (F.A. Rezende). Control patients underwent surgical treatment for nonvascular pathology (epiretinal membrane or macular hole) by the same surgeon. In an operating room setting, patients underwent surgery under local retro/peribulbar anesthesia. A 5% povidone-iodine solution was used to clean the periocular skin, and topical instillation into the eye and within the cul-de-sac was left in place for 5 minutes. Three-port 25-gauge transconjunctival pars plana vitrectomy was performed through 25-gauge valved cannulas (Alcon). Under microscope visualization using a wide-angle viewing system (Resight, Zeiss), undiluted vitreous was collected with a 25-gauge vitrector. After vitreous biopsy, the infusion line was opened, and vitrectomy and membrane
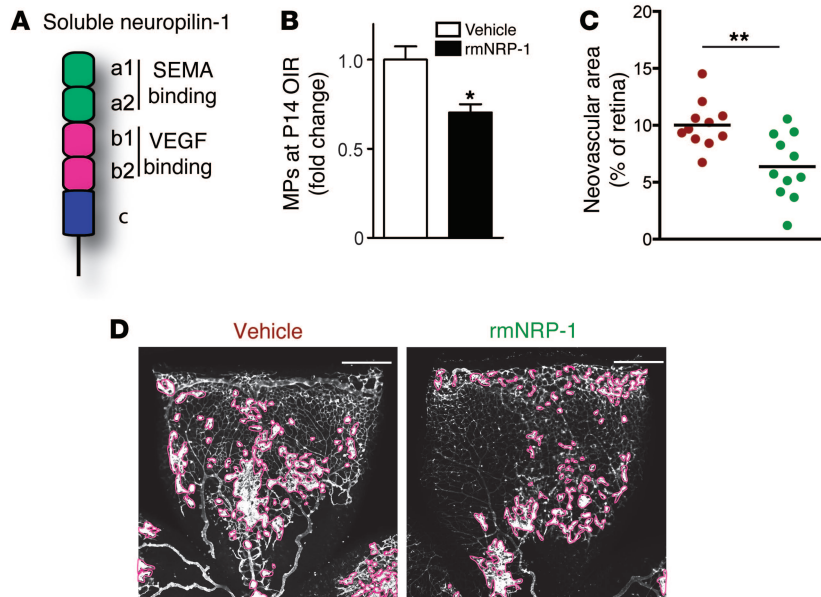
Figure 11. Therapeutic intravitreal administration of soluble NRP-1 reduces MP infiltration and pathological neovascularization in retinopathy. (A) WT mice were subjected to OIR and injected intravitreally at P12 with soluble rmNRP-1 as a trap to sequester OIR-induced ligands of NRP-1. (**B**) At P14, FACS analysis revealed a decrease of over 30% in the number of retinal MPs in rmNRP-1–injected retinas. Data are expressed as a fold change relative to control (vehicle-injected retinas) ± SEM; n = 3–4 (total of 12–16 retinas per condition; each "n" comprises 4 retinas); *$P < 0.05$. (**C** and **D**) Treatment with rmNRP-1 efficiently decreased pathological neovascularization at P17 when compared with vehicle-injected eyes. Results are expressed as percentage of neovascular area versus the whole retinal area. Horizontal bars represent mean value of percentage, and dots represent individual values; n = 11, **$P < 0.01$. Scale bars: 250 μm.

peeling was performed in the usual fashion to treat diabetic vitreous hemorrhage and tractional retinal detachment. This was followed by panretinal endolaser photocoagulation, fluid-air exchange, and intravitreal anti-VEGF injection.

Quantification of SEMA3A protein by ELISA

Vitreous samples were frozen on dry ice immediately after biopsy and stored at −80°. Samples were centrifuged at 15,000 g for 5 minutes at 4°C prior to analysis. SEMA3A levels were quantified in supernatants using ELISAs following manufacturer's instructions (USCN Life Science Inc.).

Assessment of SEMA3A protein levels by Western blot

Equal volumes of vitreous fluid (20 μl) from PDR and control patients were assessed by standard SDS-PAGE technique for the presence of SEMA3A (Abcam).

Real-time PCR analysis

RNA was isolated using the GenElute Mammalian Total RNA Miniprep Kit (Sigma-Aldrich) and digested with DNase I to prevent amplification of genomic DNA. Reversed transcription was performed using M-MLV reverse transcriptase (Life Technologies), and gene expression was analyzed using SYBR Green (Bio-Rad) in an ABI Biosystems Real-Time PCR machine. β-Actin was used as a reference gene.

Immunohistochemistry

For visualization of pan-retinal vasculature, flat-mount retinas were stained with rhodamine-labeled Griffonia (Bandeiraea) Simplicifolia Lectin I (Vector Laboratories Inc.) in 1 mM $CaCl_2$ in PBS for retinal vasculature and anti-mouse/rat NRP-1 antibody (goat IgG; R&D Systems) and IBA1 (rabbit polyclonal; Wako).

Primary peritoneal macrophages culture

Adult WT or LysM-Cre $Nrp1^{fl/fl}$ mice were anesthetized with 2% isoflurane in oxygen 2 l/min and then euthanized by cervical dislocation. Then, a small incision in abdominal skin of mouse was performed. Skin was pulled to each size of the mouse, and the peritoneal cavity

was washed with 5 ml PBS plus 3% FBS for 2 minutes. Then, the harvested cells were centrifuged for 5 minutes at 100 g, resuspended in medium (DMEM F12 plus 10% FBS and 1% streptomycin/penicillin), and plated. After 1 hour of culture at 37°C under a 5% CO_2 atmosphere, the medium was changed and cells were cultured for the next 24 hours in the same conditions before use in Transwell migration assay.

Transwell migration assay

Migration assays were performed in 24-well plates with 8-μm pore inserts. Primary peritoneal macrophages (5×10^5 cells) resuspended in 200 μl medium (DMEM F12 plus 10% FBS and 1% streptomycin/penicillin) were added to the upper chamber. 800 μl medium, with or without migratory factors, MCP-1 (100 ng/ml), SEMA3A (100 ng/ml), and $VEGF_{165}$ (50 ng/ml), was added to the lower chamber. Cells were allowed to migrate through the insert membrane overnight at 37°C under a 5% CO_2 atmosphere. In some experiments, cells were first pretreated with Y-27632 (Sigma-Aldrich), selective ROCK inhibitor (100 μg/ml), for 1 hour at 37°C. The inserts were then washed with PBS, and nonmigrating cells were swabbed from the upper surface of the insert membrane with cotton buds. Then, the membranes with migrated cells were fixed with 4% paraformaldehyde for 20 minutes, washed twice with PBS, and mounted on the slide. The cells were stained using mounting medium with DAPI (Vector Laboratories Inc.). Then, 9 random fields per each membrane were photographed using an inverted fluorescence microscope at ×20 magnification, and the cells were counted using ImageJ software.

Choroidal explants and microvascular sprouting assay

The ex vivo choroid explant analysis and quantification of microvascular sprouting were performed as described previously (57). Briefly, choroids from LysM-Cre $Nrp1^{+/+}$ and LysM-Cre $Nrp1^{fl/fl}$ mice (n = 6 for each condition) were dissected shortly after enucleating eyes. After plating segmented choroids into 24-well tissue culture plates and covering with Matrigel (BD Biosciences), samples were treated with EGM-2 medium, EGM-2 medium with PBS filled liposome, or EGM-2 medium with dichloromethylenediphosphonic acid disodium
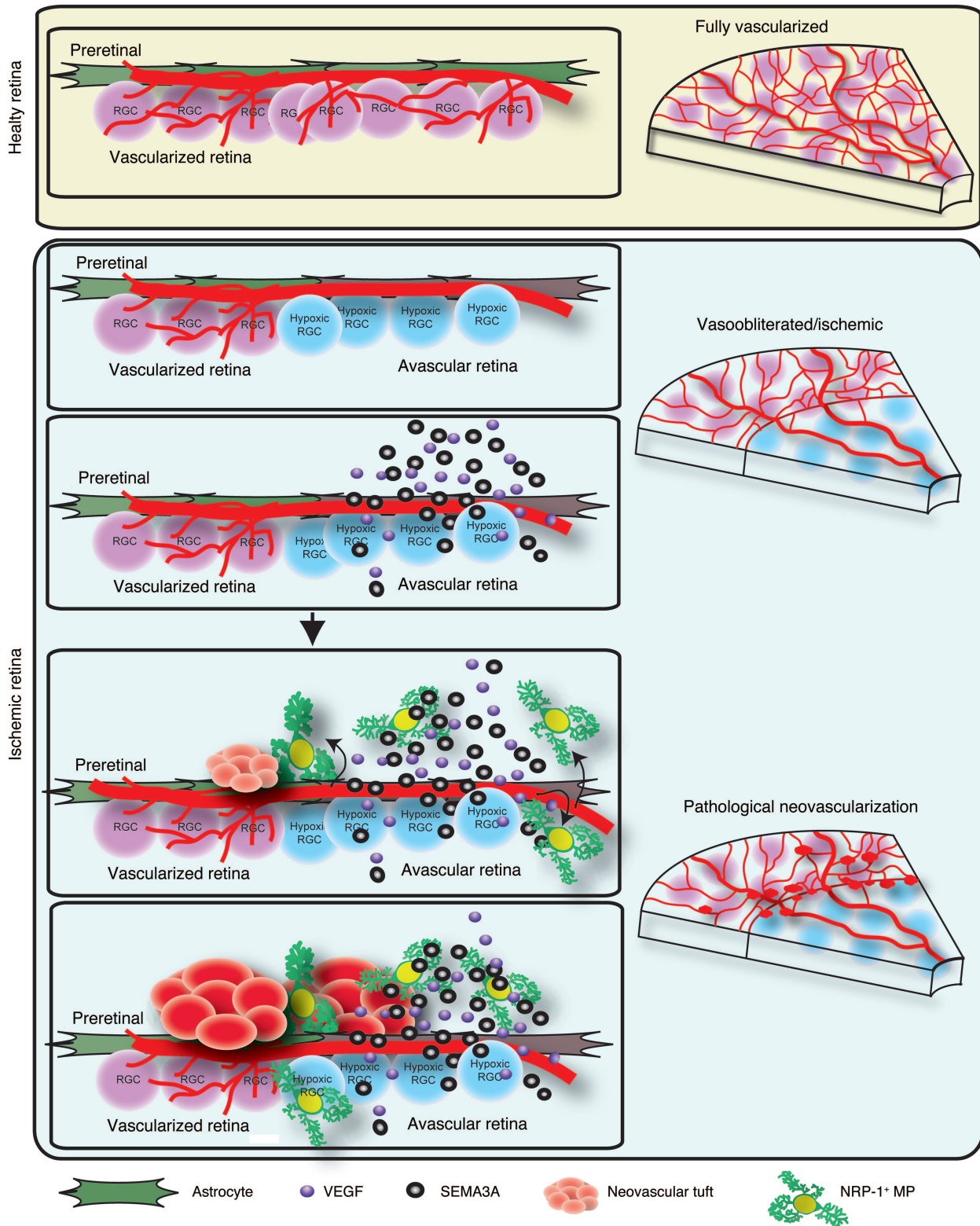
Figure 12. Schematic depiction of findings. The schematic illustrates that during ischemic retinopathies, such as diabetes, avascular zones of the retina, ischemic neurons, and neural tissue produce ligands of NRP-1 (SEMA3A and VEGF), which in turn act as potent chemoattractive agents for proangiogenic microglia. The NRP-1+ microglia then partake in the pathogenesis of proliferative retinopathy. RGC, retinal ganglion cell.

salt filled liposome (Sigma-Aldrich). The packaging of liposomes was performed according to ref. 58. Twelve hours later, liposomes containing passenger compounds were removed from the wells, followed by washing with PBS. Macrophages from primary peritoneal macrophage cultures (from either LysM-Cre $Nrp1^{+/+}$ or LysM-Cre $Nrp1^{fl/fl}$ mice) were added to choroidal explant cultures to investigate the impact of macrophages on microvascular sprouting.

Soluble recombinant NRP-1

WT mice subjected to OIR were intravitreally injected with rmNRP-1 from plasmid (29) or R&D Systems at P12.

Recombinant proteins

The following recombinant proteins were used: recombinant mouse CCL2/JE/MCP-1 (from *E. coli*) (R&D Systems) concentration used in vitro at 100 ng/ml; recombinant human SEMA3A Fc chimera (from murine myeloma cell line NS0) (R&D Systems) concentration used in vitro at 100 ng/ml; and recombinant human $VEGF_{165}$ (PeproTech) concentration used in vitro at 50 ng/ml.

Statistics

Data are presented as mean ± SEM. We used a 2-tailed Student's *t* test and ANOVA, where appropriate, to compare the different groups. $P < 0.05$ was considered statistically different. For ELISA, statistical analysis was performed using nonparametric Mann-Whitney test (GraphPad Prism).

Study approval

Human samples. We obtained approval of human clinical protocols from the Hopital Maisonneuve-Rosemont ethics committee (Ref. CER: 10059), and patients recruited for local core vitreal biopsy sampling afflicted with type 1 or type 2 diabetes mellitus provided written informed consent. The entire procedure was performed as an outpatient procedure in the minor procedure room within the ambulatory clinic of the Department of Ophthalmology at Hopital Maisonneuve-Rosemont. All instruments were opened and handled in a sterile manner. The study conforms to the tenets of the Declaration of Helsinki.

Animals. All animal studies were performed according to the Association for Research in Vision and Ophthalmology Statement for the Use of Animals in Ophthalmic and Vision Research and were approved by the Animal Care Committee of the University of Montreal in agreement with the guidelines established by the Canadian Council on Animal Care.

1. Lampron A, Elali A, Rivest S. Innate immunity in the CNS: redefining the relationship between the CNS and Its environment. *Neuron*. 2013;78(2):214–232.
2. Ousman SS, Kubes P. Immune surveillance in the central nervous system. *Nat Neurosci*. 2012;15(8):1096–1101.
3. Adamis AP, Berman AJ. Immunological mechanisms in the pathogenesis of diabetic retinopathy. *Semin Immunopathol*. 2008;30(2):65–84.
4. Antonetti DA, Klein R, Gardner TW. Diabetic retinopathy. *N Engl J Med*. 2012;366(13):1227–1239.
5. Joussen AM, et al. A central role for inflammation in the pathogenesis of diabetic retinopathy. *FASEB J*. 2004;18(12):1450–1452.
6. Ambati J, Fowler BJ. Mechanisms of age-related macular degeneration. *Neuron*. 2012;75(1):26–39.
7. Sennlaub F, et al. CCR2(+) monocytes infiltrate atrophic lesions in age-related macular disease and mediate photoreceptor degeneration in experimental subretinal inflammation in Cx3cr1 deficient mice. *EMBO Mol Med*. 2013;5(11):1775–1793.
8. Combadiere C, et al. CX3CR1-dependent subretinal microglia cell accumulation is associated with cardinal features of age-related macular degeneration. *J Clin Invest*. 2007;117(10):2920–2928.
9. Dammann O. Inflammation and retinopathy of prematurity. *Acta Paediatr*. 2010;99(7):975–977.
10. Tremblay S, et al. Systemic inflammation perturbs developmental retinal angiogenesis and neuroretinal function. *Invest Ophthalmol Vis Sci*. 2013;54(13):8125–8139.
11. Hartnett ME, Penn JS. Mechanisms and management of retinopathy of prematurity. *N Engl J Med*. 2012;367(26):2515–2526.
12. Kempen JH, et al. The prevalence of diabetic retinopathy among adults in the United States. *Arch Ophthalmol*. 2004;122(4):552–563.
13. Sapieha P, et al. Proliferative retinopathies: angiogenesis that blinds. *Int J Biochem Cell Biol*. 2010;42(1):5–12.
14. Robinson GS, et al. Nonvascular role for VEGF: VEGFR-1, 2 activity is critical for neural retinal development. *FASEB J*. 2001;15(7):1215–1217.
15. Saint-Geniez M, et al. Endogenous VEGF is required for visual function: evidence for a survival role on muller cells and photoreceptors. *PLoS One*. 2008;3(11):e3554.
16. Hellström A, Smith LE, Dammann O. Retinopathy of prematurity. *Lancet*. 2013;382(9902):1445–1457.
17. Sapieha P. Eyeing central neurons in vascular growth and reparative angiogenesis. *Blood*. 2012;120(11):2182–2194.
18. Kern TS, Barber AJ. Retinal ganglion cells in diabetes. *J Physiol*. 2008;586(pt 18):4401–4408.
19. Binet F, et al. Neuronal ER stress impedes myeloid-cell-induced vascular regeneration through IRE1α degradation of netrin-1. *Cell Metab*. 2013;17(3):353–371.
20. Cerani A, et al. Neuron-derived semaphorin 3A is an early inducer of vascular permeability in diabetic retinopathy via neuropilin-1. *Cell Metab*. 2013;18(4):505–518.
21. Joyal JS, et al. Ischemic neurons prevent vascular regeneration of neural tissue by secreting semaphorin 3A. *Blood*. 2011;117(22):6024–6035.
22. Checchin D, Sennlaub F, Levavasseur E, Leduc M, Chemtob S. Potential role of microglia in retinal blood vessel formation. *Invest Ophthalmol Vis Sci*. 2006;47(8):3595–3602.
23. Connor KM, et al. Increased dietary intake of omega-3-polyunsaturated fatty acids reduces pathological retinal angiogenesis. *Nat Med*. 2007;13(7):868–873.
24. Sapieha P, et al. 5-Lipoxygenase metabolite 4-HDHA is a mediator of the antiangiogenic effect of ω-3 polyunsaturated fatty acids. *Sci Transl Med*. 2011;3(69):69ra12.
25. Stahl A, et al. Short communication: PPAR gamma mediates a direct antiangiogenic effect of omega 3-PUFAs in proliferative retinopathy. *Circ Res*. 2010;107(4):495–500.
26. Smith LE, et al. Oxygen-induced retinopathy in the mouse. *Invest Ophthalmol Vis Sci*. 1994;35(1):101–111.
27. Lee P, Goishi K, Davidson AJ, Mannix R, Zon L, Klagsbrun M. Neuropilin-1 is required for vascular development and is a mediator of VEGF-dependent angiogenesis in zebrafish. *Proc Natl Acad Sci U S A*. 2002;99(16):10470–10475.

28. Gluzman-Poltorak Z, Cohen T, Shibuya M, Neufeld G. Vascular endothelial growth factor receptor-1 and neuropilin-2 form complexes. *J Biol Chem*. 2001;276(22):18688–18694.

29. Mamluk R, Gechtman Z, Kutcher ME, Gasiunas N, Gallagher J, Klagsbrun M. Neuropilin-1 binds vascular endothelial growth factor 165, placenta growth factor-2, and heparin via its b1b2 domain. *J Biol Chem*. 2002;277(27):24818–24825.

30. Soker S, Takashima S, Miao HQ, Neufeld G, Klagsbrun M. Neuropilin-1 is expressed by endothelial and tumor cells as an isoform-specific receptor for vascular endothelial growth factor. *Cell*. 1998;92(6):735–745.

31. Fantin A, et al. Tissue macrophages act as cellular chaperones for vascular anastomosis downstream of VEGF-mediated endothelial tip cell induction. *Blood*. 2010;116(5):829–840.

32. Carrer A, et al. Neuropilin-1 identifies a subset of bone marrow Gr1- monocytes that can induce tumor vessel normalization and inhibit tumor growth. *Cancer Res*. 2012;72(24):6371–6381.

33. Casazza A, et al. Impeding macrophage entry into hypoxic tumor areas by Sema3A/Nrp1 signaling blockade inhibits angiogenesis and restores antitumor immunity. *Cancer Cell*. 2013;24(6):695–709.

34. Ritter MR, Banin E, Moreno SK, Aguilar E, Dorrell MI, Friedlander M. Myeloid progenitors differentiate into microglia and promote vascular repair in a model of ischemic retinopathy. *J Clin Invest*. 2006;116(12):3266–3276.

35. Stahl A, et al. Postnatal weight gain modifies severity and functional outcome of oxygen-induced proliferative retinopathy. *Am J Pathol*. 2010;177(6):2715–2723.

36. Clausen BE, Burkhardt C, Reith W, Renkawitz R, Forster I. Conditional gene targeting in macrophages and granulocytes using LysMcre mice. *Transgenic Res*. 1999;8(4):265–277.

37. Mattapallil MJ, et al. The Rd8 mutation of the Crb1 gene is present in vendor lines of C57BL/6N mice and embryonic stem cells, and confounds ocular induced mutant phenotypes. *Invest Ophthalmol Vis Sci*. 2012;53(6):2921–2927.

38. Klebanov O, Nitzan A, Raz D, Barzilai A, Solomon AS. Upregulation of Semaphorin 3A and the associated biochemical and cellular events in a rat model of retinal detachment. *Graefes Arch Clin Exp Ophthalmol*. 2009;247(1):73–86.

39. Koppel AM, Raper JA. Collapsin-1 covalently dimerizes, and dimerization is necessary for collapsing activity. *J Biol Chem*. 1998;273(25):15708–15713.

40. Kubota Y, et al. M-CSF inhibition selectively targets pathological angiogenesis and lymphangiogenesis. *J Exp Med*. 2009;206(5):1089–1102.

41. Okuno Y, Nakamura-Ishizu A, Kishi K, Suda T, Kubota Y. Bone marrow-derived cells serve as proangiogenic macrophages but not endothelial cells in wound healing. *Blood*. 2011;117(19):5264–5272.

42. Neufeld G, Kessler O. The semaphorins: versatile regulators of tumour progression and tumour angiogenesis. *Nat Rev Cancer*. 2008;8(8):632–645.

43. Worthylake RA, Burridge K. RhoA and ROCK promote migration by limiting membrane protrusions. *J Biol Chem*. 2003;278(15):13578–13584.

44. Dammann O, et al. Immaturity, perinatal inflammation, and retinopathy of prematurity: a multi-hit hypothesis. *Early Hum Dev*. 2009;85(5):325–329.

45. Kastelan S, Tomic M, Gverovic Antunica A, Salopek Rabatic J, Ljubic S. Inflammation and pharmacological treatment in diabetic retinopathy. *Mediators Inflamm*. 2013;2013:213130.

46. Silva PS, Cavallerano JD, Sun JK, Aiello LM, Aiello LP. Effect of systemic medications on onset and progression of diabetic retinopathy. *Nat Rev Endocrinol*. 2010;6(9):494–508.

47. Miao HQ, Soker S, Feiner L, Alonso JL, Raper JA, Klagsbrun M. Neuropilin-1 mediates collapsin-1/semaphorin III inhibition of endothelial cell motility: functional competition of collapsin-1 and vascular endothelial growth factor-165. *J Cell Biol*. 1999;146(1):233–242.

48. Klagsbrun M, Eichmann A. A role for axon guidance receptors and ligands in blood vessel development and tumor angiogenesis. *Cytokine Growth Factor Rev*. 2005;16(4):535–548.

49. Guttmann-Raviv N, Shraga-Heled N, Varshavsky A, Guimaraes-Sternberg C, Kessler O, Neufeld G. Semaphorin-3A and semaphorin-3F work together to repel endothelial cells and to inhibit their survival by induction of apoptosis. *J Biol Chem*. 2007;282(36):26294–26305.

50. Neufeld G, Sabag AD, Rabinovicz N, Kessler O. Semaphorins in angiogenesis and tumor progression. *Cold Spring Harb Perspect Med*. 2012;2(1):a006718.

51. Bussolino F, Valdembri D, Caccavari F, Serini G. Semaphoring vascular morphogenesis. *Endothelium*. 2006;13(2):81–91.

52. Yancopoulos GD. Clinical application of therapies targeting VEGF. *Cell*. 2010;143(1):13–16.

53. Miloudi K, Dejda A, Binet F, Lapalme E, Cerani A, Sapieha P. Assessment of vascular regeneration in the CNS using the mouse retina. *J Vis Exp*. 2014;(88):e51351.

54. Sapieha P, et al. Retinopathy of prematurity: understanding ischemic retinal vasculopathies at an extreme of life. *J Clin Invest*. 2010;120(9):3022–3032.

55. Stahl A, et al. The mouse retina as an angiogenesis model. *Invest Ophthalmol Vis Sci*. 2010;51(6):2813–2826.

56. Stahl A, et al. Computer-aided quantification of retinal neovascularization. *Angiogenesis*. 2009;12(3):297–301.

57. Shao Z, et al. Choroid sprouting assay: an ex vivo model of microvascular angiogenesis. *PLoS One*. 2013;8(7):e69552.

58. van Rooijen N, van Kesteren-Hendrikx E. "In vivo" depletion of macrophages by liposome-mediated "suicide". *Methods Enzymol*. 2003;373:3–16.